Mesoporous Silicon Negative Electrode for Thin Film Lithium-Ion Microbatteries

Erwann Luais, Fouad Ghamouss, Jérôme Wolfman, Sébastien Desplobain, Gael Gautier, François Tran-Van, Joe Sakai

Mesoporous Silicon Negative Electrode for Thin Film Lithium-Ion Microbatteries

Erwann Luais,[a,b] Fouad Ghamouss,[b,*] Jérôme Wolfman,[a] Sébastien Desplobain,[c] Gaël Gautier,[a] François Tran-Van,[b] Joe Sakai,[a]

[a] Groupe de Recherche En Matériaux, Microélectronique, Acoustique et Nanotechnologies (GREMAN), UMR 7347, CNRS / Université François Rabelais de Tours, Parc de Grandmont, 37200 Tours, France

[b] Laboratoire de Physico-Chimie des Matériaux et des Electrolytes pour l'Energie (PCM2E), EA 6299, Université François Rabelais, Parc de Grandmont, 37200 Tours, France

[c] SiLiMiXT, 10 rue de Thalès de Milet, CS 97155, 37071 Tours Cedex 2, France

*corresponding author : fouad.ghamouss@univ-tours.fr

Abstract

A mesoporous silicon film (5 µm thick, diameter of pores ranging from 60 to 70 nm) was prepared through electrochemical etching of a silicon wafer, and its performance as a negative electrode for lithium-ion batteries was studied. Cyclic voltammetry measurements showed a sluggish penetration of the electrolyte into the pores along the depth, raising lithiation and delithiation peaks during scanning. The penetration of the electrolyte was monitored by elemental analysis in the mesoporous layer with energy-dispersive X-ray spectroscopy coupled with scanning electron microscopy. As the electrolyte decomposes forming lithium carbonate, fluorine and phosphorus moieties, these chemical compounds tag the part of the porous layer involved in the lithiation-delithiation processes. After 50 voltammetric cycles, the electrochemical reaction took place in the whole depth of the porous silicon layer. In contrast, after only 10 cycles, the bottom part of the silicon pores was not affected. Galvanostatic cycling at a rate of 300 µA cm^{-2} was performed for two different lower cut-off voltages. A charge limitation of 0.1 V resulted in a stable specific capacity of 1910 mAh g^{-1}. For a deeper charge with a potential limitation of 0.07 V, a higher specific capacity of 2480 mAh g^{-1} was reached but unfortunately accompanied by a severe fading of the

performances. This phenomenon was attributed to the strong mechanical damages in the porous structure of the silicon negative electrode. Electrochemically-prepared mesoporous silicon layer was confirmed to act as a negative electrode with high capacity for lithium-ion microbatteries.

Keywords

Mesoporous Silicon, Silicon-based negative electrode, Lithium-Ion Batteries, Microbatteries

1. Introduction

Direct integration of batteries for nomad electronic devices is challenging in regards to the miniaturization of biomedical implants, sensors or integrated circuits. Hence, on-board rechargeable batteries with small dimensions and high energy storage density are required [1, 2]. The microbattery integration would be easier if the active layers fabrication methods are compatible with silicon technology. Due to its high theoretical gravimetric capacity of 3579 mAh g^{-1} at room temperature, silicon (Si) is a promising negative electrode material for Li-ion microbatteries with high energy density. However, the use of Si-based negative electrodes is accompanied by a major problem consisting of its high volume expansion during charging. This volumetric expansion leads to mechanical damages (pulverization and cracking) of the Si layer [3-8]. In order to prevent this issue, nanostructured Si materials such as nanotubes [9], nanowires [10] or nanoparticles [11] have been developed. In order to facilitate the integration of microbatteries with Si-based negative electrodes, it is desirable to directly nanostructure the surface of a Si wafer. Electrochemical etching of Si wafer is a reliable way to obtain Porous Si with controled nanometer-sized dimensions. Thakur *et al.* proposed the preparation of a negative electrode based on electrochemically-etched macroporous Si. They demonstrated that a thin gold coating of the porous Si layer enhances both its capacity and its retention [12]. Sun *et al.* used a self-supported macroporous Si layer prepared through an entire electrochemically-assisted process as a

negative electrode [13]. Shin *et al.* electrochemically-etched a Si wafer to prepare a macroporous Si negative electrode [14]. This work was extended in the same research group by Kang *et al.* in preparing micro-nano-hybrid porous structure from an electrochemically-etched Si wafer [15]. As a negative electrode for Li-ion batteries, the authors showed minimal mechanical damages even after 50 voltammetric cycles [15]. The Si-based negative electrodes presented in these precedent works are based on an architecture comprising a macroporous structure formed by etching a supporting initial single crystal Si wafer. The presence of this underneath Si waferwould lead to some lifetime issues related to the cycling stability. Indeed, pulverization and cracking of the overall electrode material could be promoted by the lithiation and delithiation of the supporting Si wafer. Moreover, , the real fraction or part of the Si material (from porous Si layer and from bulk supporting Si wafer) involved in the electrochemical reactions could remain uncertain.

In this paper, mesoporous silicon is used as negative electrodes for Li-ion batteries. The electrode architecture is based on a mesoporous Si layer directly prepared on a Si wafer through its electrochemical etching. We aim to demonstrate if the supporting bulk Si wafer does or does not participate in the lithiation and delithiation reactions. Morphological characterizations of the porous Si surface and cross section were performed by scanning electron microscopy (SEM). Cyclic voltammetry (CV) and energy-dispersing x-ray spectroscopy (EDX) were carried out to monitor the impregnation of the electrolyte through the porous layer. Moreover, the charge-discharge induced mechanical damages in the porous Si were observed using various galvanostatic cycling at different current rates and for different cut-off voltages

2. Experimental

2.1 Preparation of mesoporous silicon

The porous silicon (pSi) layer was prepared in a 30 wt. % HF/H_2O acid electrolyte added with 350 ppm TritonX-100 surfactant from Aldrich®. The starting material was a (100)-

oriented silicon wafer, p-type doped with a resistivity of 2-4 mΩ cm. The pSi etching was performed in a double-tank electrochemical cell. The anodic polarization of the wafer was assumed by a backside electrolytic contact. This electrolytic contact and the p^+ doping of the wafer ensured a homogeneous potential distribution. To achieve a mesoporous layer of 5 µm-thick, a current density of 400 mA cm^{-2} was applied for 30 s. This high current density remains lower than the J_{PS} value (630 mA/cm^2) which defines the erosion limit [16]. We have selected a highly-doped wafer (above 10^{19} cm^{-3}) in addition to the high current density to produce large mesopores in p-type silicon [17]. The pore diameter with present conditions was expected to be larger than 20 nm.

2.2 Characterizations

Electrochemical half-cells were prepared in an argon-filled glovebox (water and dioxygen contents below 10 ppm) within the form of 2032 two electrodes coin cells where the working electrodes were dried pSi shards and the counter electrodes were lithium foils. The working and the counter electrodes were separated with a polypropylene membrane (Celgard® 2400) and a glass microfiber membrane (Whatman® GF/C) impregnated with 1 M $LiPF_6$ dissolved in a 1:1 (v/v) mixture of ethylene carbonate (EC, Sigma-Aldrich®) and dimethylcarbonate (DMC, Sigma-Aldrich®). Cyclic voltammograms (CVs) were recorded at a scan rate of 0.1 mV s^{-1} between 0.02 and 2 V versus Li/Li^+. Galvanostatic cycling was performed at different current densities and for different cut-off voltages as detailed in the results section. All electrochemical measurements were made with a Biologic® VMP3.

SEM imaging was performed in a dual beam FIB STRATA 400 from FEI equipped with an EDX INCA set-up from OXFORD instrument. Compositions in the stack at various locations were locally evaluated on cross-sections with EDX.

3. Results and discussions

Cross-sectional SEM images of the mesoporous silicon negative electrodes studied in this work are presented in Figure 1. Déjà dit plus haut. The pores diameter was found to

range from 60 to 70 nm (Figure 1-b), and from a classical gravimetric method this mesoporous layer presents a porosity between 55 and 60 %. The mass of pSi, estimated to be 0.76 mg cm^{-2}, is the only one. used to determine specific capacities.

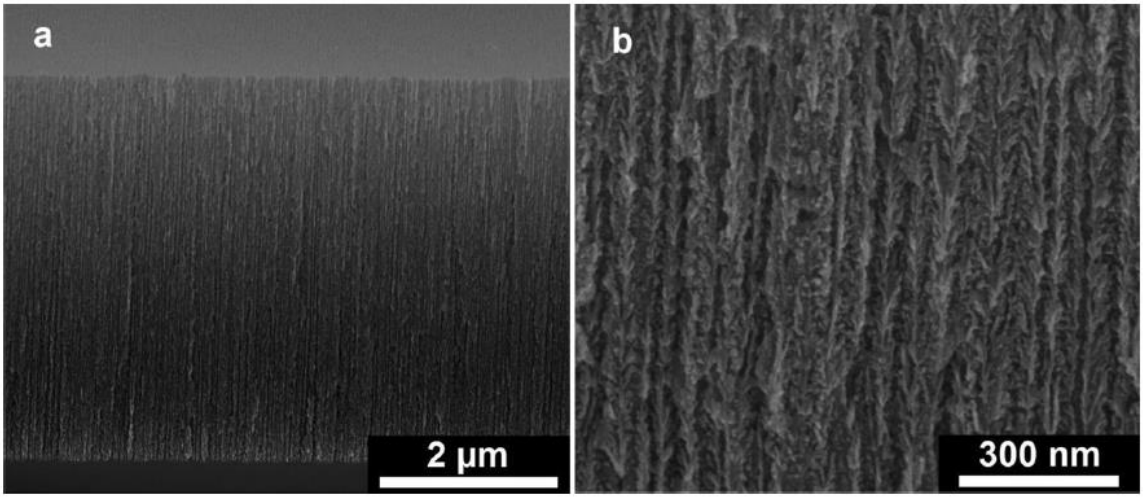

Fig. 1. Cross-sectional SEM images of a mesoporous Si wafer in (a) low magnification and (b) high magnification.

Figure 2 shows CVs performed in EC/DMC containing 1 M $LiPF_6$ between 0.02 and 2 V vs Li/Li^+ at a scan rate of 0.1 mV/s. Figure 2-a displays the potential region where two first irreversible reactions occurred on as-prepared mesoporous Si (bold curve). These cathodic reactions were observed on the first cycle, exhibiting cathodic peaks located at 1.35 and 1.1 V versus Li/Li^+. These two first waves could be attributed to the reduction of adventitious contaminations, or to water traces or to Si oxide species [18-20]. For comparison, we treated a sample of mesoporous Si with 2.5% HF for 90 s to remove parts of Si oxides at the pSi surface. The CV curve of this HF-treated sample (control sample) is shown in Figure 2-a as a dashed curve. It was observed that cathodic peaks for these irreversible reactions mainly diminished for the control sample, suggesting that these reactions may correspond to the electrochemical reduction of Si oxides. On as-prepared mesoporous Si (without HF pretreatment), another irreversible reaction was observed at a potential of 0.65 V vs Li/Li^+ (Figure 2-b). This cathodic peak would correspond to the irreversible electrolyte reduction and the solid electrolyte interface (SEI) formation [20-23]. It is worth noting for as-prepared

mesoporous Si that these three peaks corresponding to irreversible reactions (cathodic reductions of SiO_x and electrolyte) were totally suppressed on the consecutive scans (Figure 2-b). Figure 2-c shows the CVs from 1st to 50th scans where the intensity of the cathodic peak attributed to the lithiation of Si phases increases upon scanning (Figure 2-c) [13-15, 22, 24, 25]. On the reverse scans, anodic peaks located at potentials of 0.41 and 0.53 V in the 50th scan would be attributed to the delithiation reactions of Li-Si phases [13-15, 22, 24, 25]. The increase of the peak intensities suggests the increase of the Si amount involved in lithiation and delithiation reactions. During 50 scans, the Li penetrated deeper in the mesoporous Si, raising the cathodic peak intensity.This intensity then stabilized for the subsequent scans (Figure 2-d). This current intensity stabilization, attributed to the lithiation of amorphous Si phases, would suggest that only the Si within the porous layer is involved in the electrochemical reactions.

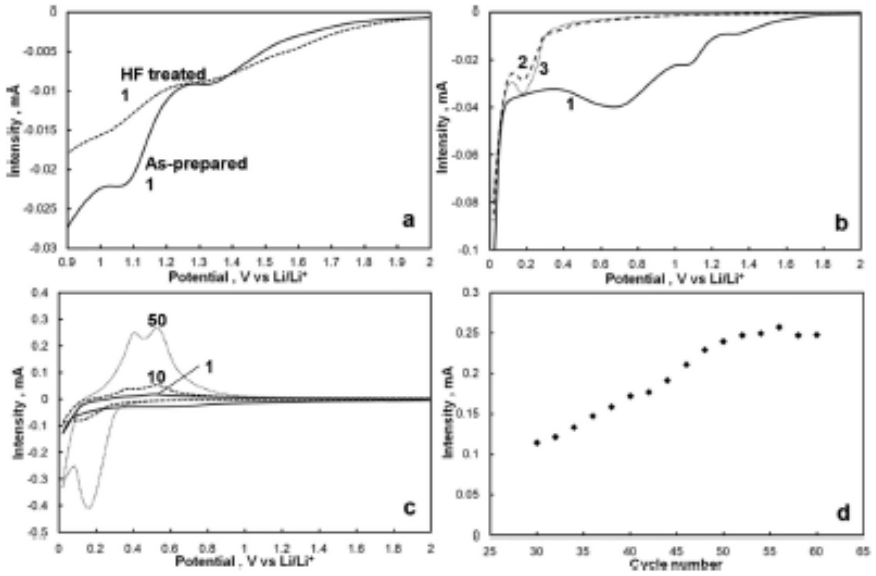

Fig. 2. Cyclic voltammograms of pSi negative electrodes in EC/DMC + 1 M $LiPF_6$ at a scan rate of 0.1 mV s^{-1}. (a) 1st cycle for pSi material with native oxide (bold curve) and for pSi after a HF treatment (dashed curve). (b) 1st cycle (bold curve), 2nd cycle (dashed curve) and 3rd cycle (dotted curve) for an as-prepared sample. (c) 1st cycle (bold curve), 10th cycle (dashed curve), and 50th cycle (dotted curve) for an as-prepared sample. (d) Peak intensity of the cathodic peak related to the lithiation of pSi.

Figure 3-a displays CVs recorded at the 10th, 15th, 20th and 30th scans. The reverse scans show anodic peaks attributed to the delithiation reactions of Li-Si phases [13-15]. These peaks are located at potential values very close to the one found for the 50th scan (Figure 2-c). The potential of the first peak is comprised in a potential range from 0.38 V (for

the 10th scan) to 0.40 V (30th scan), and the second peak at higher potentials is comprised between 0.52 V (10th scan) to 0.53 V (25th scan). Cathodic peaks were thoroughly monitored between the 10th and the 30th cycles, where the voltammograms showed different profiles for the cathodic peak attributed to the Si lithiation reactions (Figure 3-b). For cycles from 10th to 22nd, a peak is located at a potential around 0.1 V and would be relative to the lithiation of crystalline silicon [24-27]. The disappearance trend of this peak through cycling suggests that less and less crystalline Si would be affected by the lithiation reaction. In the 10th cycle this cathodic peak was single, whereas a second cathodic peak appeared closer to 0.2V in subsequent cycles. This second peak would be attributed to lithiation reactions of amorphous Si phases [24-27]. From works published in literature, the peak attributed to the lithiation of crystalline Si usually disappears after the first cycle, in contrast to our mesoporous structure where this peak remains even after 22 cycles. This observation would suggest that the lithiation would occur on crystalline Si unaffected by previous lithiations from thepreceding cycle. Therefore, we suspect a sluggish (progressive) penetration of the electrolyte through the mesoporous structure, allowing for a first electrolyte- unaffected Si contact even after a few cycles. This second peak disappeared after 22 cycles of lithiation/delithiation reactions, suggesting that the whole mesoporous structure have been already converted into amorphous phases during precedent cycles. This observation supports our hypothesis that the underneath single crystalline Si is not involved during lithiation/delithiation reactions.??? Et si au contraire une couche de Si du wafer a été convertie en Si amorphe avec une épaisseur telle que le Li ne peut plus diffuser au travers pour atteindre du Si cristallin en dessous? Est ce que cela ne donnerait pas le même résultat?

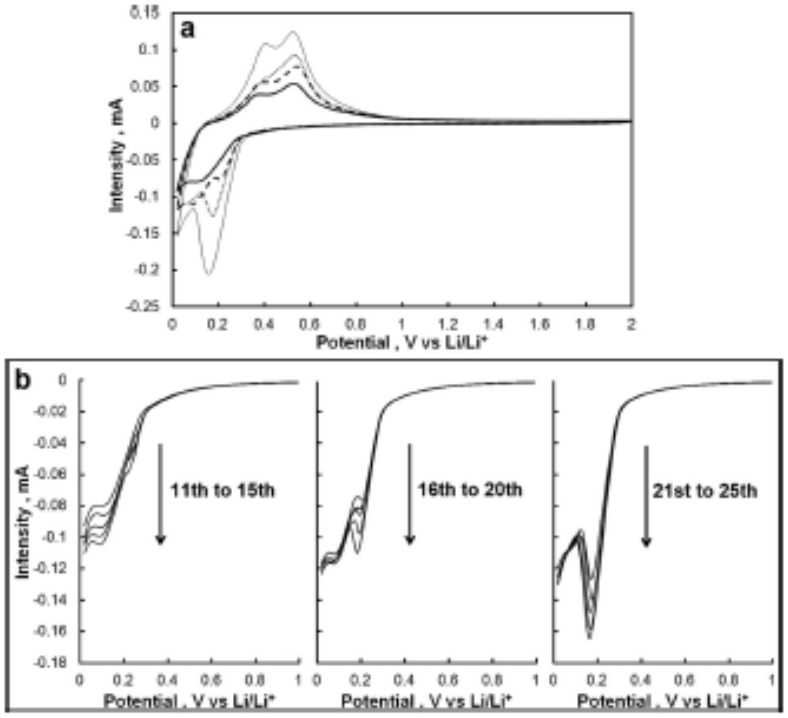

Fig 3. Cyclic voltammograms of a pSi negative electrode in EC/DMC + 1 M $LiPF_6$ at a scan rate of 0.1 mV s^{-1}. (a) 10th cycle (bold continuous curve), 15th cycle (dashed curve), 20th cycle (dotted curve) and 30th cycle (thin continuous curve). (b) 11th to 25th cycles in a potential window from 0.02 to 1 V.

To follow what is occurring during the penetration of electrolyte, SEM and EDX analyses were performed for Si negative electrodes after lithiation-delithiation cycles. Figure 4-a shows a SEM image in tilted view of a pSi after 10 consecutive cycles. On the SEM image, the surface of the pSi is labeled as (i). Between the surface and the bulk Si, we distinguished two regions with two distinct morphologies in the porous layer after first 10 cycles. The first region (ii) is the thicker part of the porous layer and the second region (iii) is the bottom of the pSi. We suggest that these two regions are present due to the slow penetration of the electrolyte inside the mesopores. During the first 10 cycles, only a part of the pSi is involved in the lithiation-delithiation process, resuming the observation established from Figures 2 and 3. Hence, there is an increase of the intensity of peaks attributed to the phenomena of both lithiation and delithiation of silicon. From the first CV, we therefore observed the liquid electrolyte impregnation in the mesoporous layer raising the intensity of these peaks. To assess this hypothesis we performed SEM-EDX characterization (Figure 4-b). For comparison, the EDX spectrum of the pSi surface after 10 cycles is shown in Figure 4-b-i. The EDX spectrum shows the presence of Si, O, C and also the noteworthy presence

of P and F. The presence of carbon, phosphorous and fluorine should be due to electrolyte decomposition to form the SEI composed of PEO (Polyethylene oxide) oligomers, Li_2CO_3, LiF and $LiPF_6$ and Li_xPF_y [18, 21]. We suggest that the presence of regions (ii) and (iii) is due to a gradient in the electrolyte penetration. This hypothesis would be supported by the EDX observation achieved on these two different regions. Indeed, EDX spectrum from region (ii) (main part of the pSi affected by the cycling) reveals the presence of Si, C and O, and also the presence of P and F. The presence of the last two elements would suggest that electrolyte decomposition could occur in this part of the pSi. In contrast, on the EDX spectrum at the bottom of the pores (Figure 4-b-iii), phosphorous and fluorine are absent, suggesting that there is no electrolyte decomposition in this part of the pSi. This observation would support that the liquid electrolyte did not reach the bottom part of the porous layer after only 10 cycles. As the electrolyte would not affect the whole porous layer, the peaks associated to lithiation and delithiation of Si are limited in their intensity.

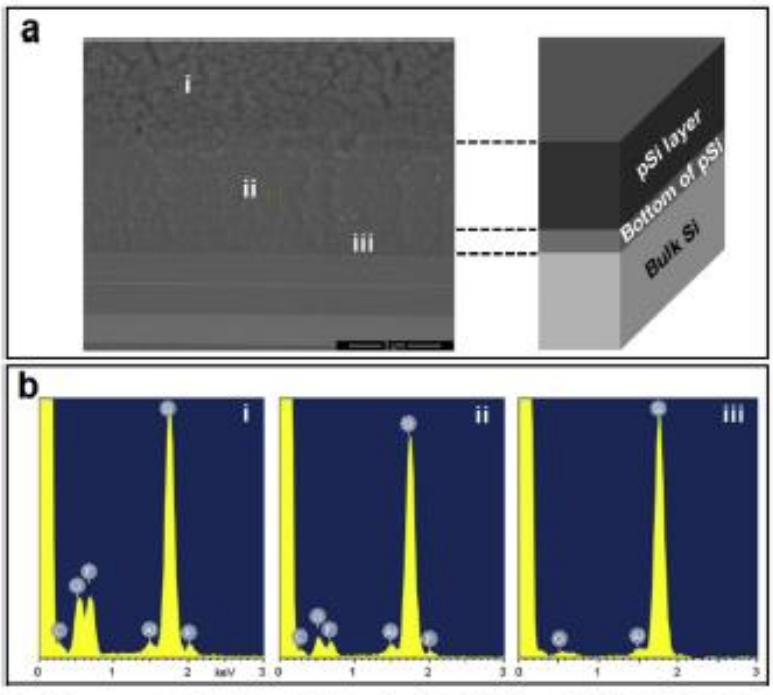

Fig. 4. (a) SEM image in a tilted view of the mesoporous Si after 10 cycles with (i) the surface of the pSi (ii) main part of pSi affected by the electrolyte penetration for 10 CVs (iii) pSi part unaffected by the electrochemical reactions. Schematic of regions in the SEM image is shown on the right. (b) EDX spectra collected from the (i) pSi surface, (ii) main part of the pSi and (iii) bottom of the pSi pores.

Figure 5-a shows a tilted SEM view of a pSi sample after performing voltammetry for 50 cycles. The region labelled as (i) is the surface of the pSi negative electrode, while the

region (ii) is the main part of the pSi layer. We attributed the region (iii) to the bottom of the pores. EDX spectra for each region are displayed in Figure 5-b. Regions (i), the surface, and (ii), the main part of the pSi layer, present a very close chemical composition with the presence of P and F, as well as Si, O and C. In contrast to the sample which underwent 10 voltammetric cycles, fluorine is present in region (iii), the bottom of the pores. This observation suggests that, for 50 cycles, the electrolyte could reach the bottom of the pSi layer and therefore the whole porous silicon layer acted as the active material of the electrode. Thus, the liquid electrolyte penetrated deeper inside the porous layer after 50 cycles, raising the intensities of peaks associated to lithiation and delithiation of silicon. From EDX analysis of region (ii) of the mesoporous layer, we showed that the nature of the SEI evolved during cycling. Indeed comparing the spectrum in region (ii) for samples cycled 10 times (Figure 4) and 50 times (Figure 5), it can be seen that there is a higher concentration of carbon and oxygen elements due to formation of Li carbonates species in the 50 cycles sample. It is known that these compounds dominate the SEI composition on Si materials through cycling [21]. This would mean that the mesopores may not be fully clogged, leading to a possible electrolyte diffusion after 10 or 50 cycles???. This means that the SEI can evolve during the electrolyte penetration in the pores. EDX analysis of the region (iii) of the mesoporous layer highlights that the electrochemical reactions are constrained in the porous layer, and so the underneath bulk Si wafer is not participating into these reactions.

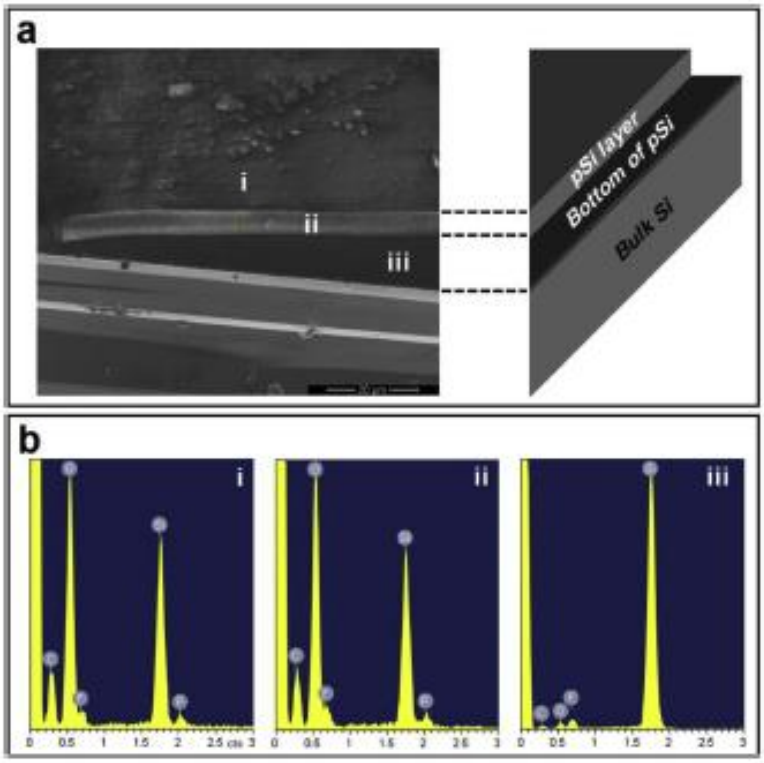

Fig. 5. (a) SEM image in a tilted view of the mesoporous Si after 50 cycles with (i) the surface of the pSi (ii) main part of pSi layer (iii) bottom of the porous layer. Schematic of regions in the SEM image is shown on the right. (b) EDX spectra achieved from the (i) pSi surface, (ii) main part of the pSi and (iii) bottom of the pSi.

It is known that the chemical reactions and mechanical feedback through lithiation and delithiation processes in Si negative electrodes drastically depend on their cut-off potentials. Cui *et al.* showed that Si nanowires became totally amorphous for a low cut-off voltage of 10 mV for the charge (alloying) whereas Si nanowires kept a crystalline phase in the cores when this potential was 150 mV [27]. Laik *et al.* also showed that the capacity retention is strongly degraded by too low cut-off voltages , with an optimal value of 100 mV corresponding to the highest capacity retention [26]. Due to the formation of $Li_{15}Si_4$ phase during the alloying charge for cut-off voltages lower than 100 mV, the cycling life is low [26]. Green *et al.* showed that modifying the lower cut-off voltages to a higher charge depth lead to an increase of the volume expansion of Si pillars during alloying and even promoted cracks formation of the underlying bulk Si [4]. Obrovac *et al.* showed that better cycling performance are obtained when the low cut-off voltage is maintained above 50 mV, and that lithiated amorphous silicon could crystallize at 50 mV to form $Li_{15}Si_4$ [28]. In the present study, all galvanostatic cycling were performed at a current density of 50 µA cm^{-2} (~ C/50) for the

first 10 lithiation/delithiation cycles, namely an activation step. We found that this activation step with a low current density, is necessary for the mesoporous silicon material, similar to what Shin *et al.* reported for macroporous Si [14]. The cut-off voltages were set at 0.1 V for the lower limitation and 2 V for the upper limitation during the activation step. For the subsequent cycles, the cut-off potentials and the current densities were varied.

Figure 6 shows the galvanostatic profile collected with a lower cut-off voltage of 0.07 V, an upper limit of 2 V and a current density of 300 µA cm^{-2} (~ C/9) after the 11th cycle. In these conditions, we observed that the capacity quickly reached a high value close to 2480 mAh g^{-1} after 30 charge-discharge cycles. This high value of capacity, however, could not be kept through cycling, and a fading behavior was observed for the subsequent 100 cycles. The capacity at the 135th cycle was 296 mAh g^{-1}.

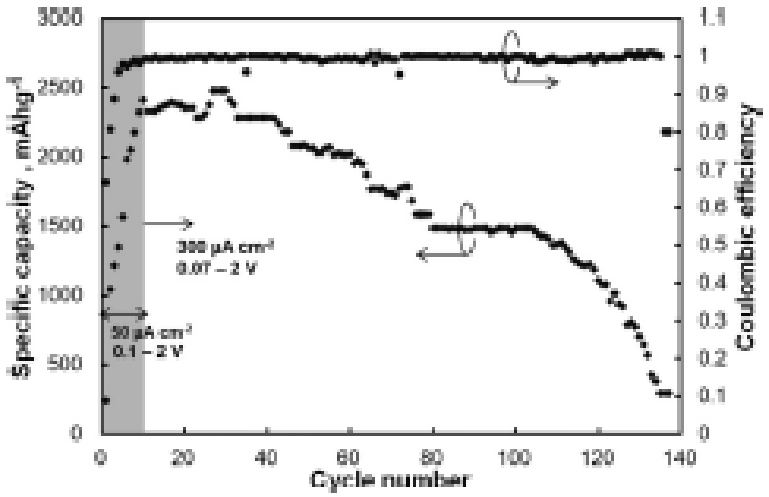

Fig. 6. Galvanostatic profiles of specific capacities (diamonds) and coulombic efficiency (circles) for a Li/pSi half-cell with cut-off voltages of 0.07 V and 2 V.

Post-mortem SEM observations were performed for this sample and we observed at low magnification that the mesoporous layer presented a huge amount of cracks (Figure 7-a). At a higher magnification (Figure 7-b and 7-c), a major part of the porous layer seemed to remain unbroken, whereas part of the top layer peeled off. Even on the mesoporous Si negative electrodes, the mechanical reactions through lithiation and delithiation processes would strongly depend on the cut-off potentials. It is worth to note that the fading behaviour

in this potential range came from the cracking of the porous layer itself and not from cracking and pulverization of the underneath Si wafer.

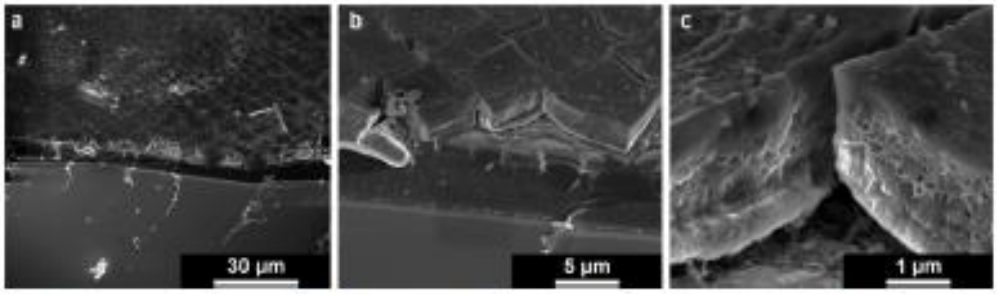

Fig. 7. SEM observations at different magnifications of a pSi sample after 150 galvanostatic cycles at 300 µA cm^{-2} with cut-off voltages of 0.07 V and 2 V.

Therefore, controlling the lithiation reaction by increasing the lower cut-off voltage would enhance the stability of the pSi negative electrode during cycling. Indeed, we demonstrate a higher stability by setting the lower potential to 0.1 V (Figure 8) instead of 0.07 V in the previous experiment (Figure 6). It is worth to note that the same activation step was reproduced here: 10 cycles at a current density of 50 µA cm^{-2} with potential limitations of 0.1 V for the lower cut-off and 2 V for the upper limit (Figure 8). At this rate, the capacity increased through cycling to reach a specific capacity of 2410 mAh g^{-1} for the 10th cycle. Once this activation step was completed, the current density was set up to 300 µA cm^{-2} (~ C/9) with cut-off potentials of 0.1 V and 2 V. At these current rate and potential limits, the capacity was initially 1910 mAh g^{-1}, and remained quite stable to the 70th cycle with a capacity of 1860 mAh g^{-1}. Cycling farther, the capacity retention dropped with a specific capacity of 1485 mAh g^{-1} for the 150th cycle. For this stability run, coulombic efficiencies were above 97 %.

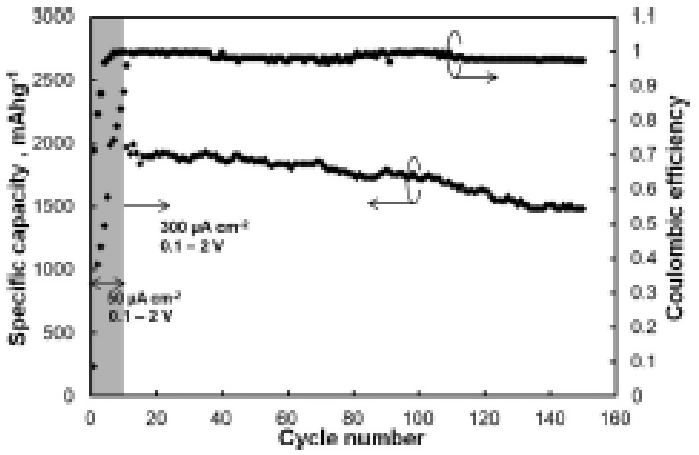

Fig. 8. Galvanostatic profiles of specific capacities (diamonds) and coulombic efficiency (circles) for a Li/pSi half-cell with cut-off voltages of 0.1 V and 2 V.

Figure 9 displays post-mortem SEM images of this sample after 150 cycles at 300 µA cm^{-2}. Figure 9-a shows at a low magnification the preserved integrity of the mesoporous Si. At a higher magnification (Figure 9-b) the mesoporous morphology remains without any peeled part, in contrast to the case of cut-offs of 0.07 V and 2 V (Figure 7). Some fractures are observed on the underlying bulk Si but it is due to the cleavage of the sample for preparing the SEM observations (Figure 9-c).

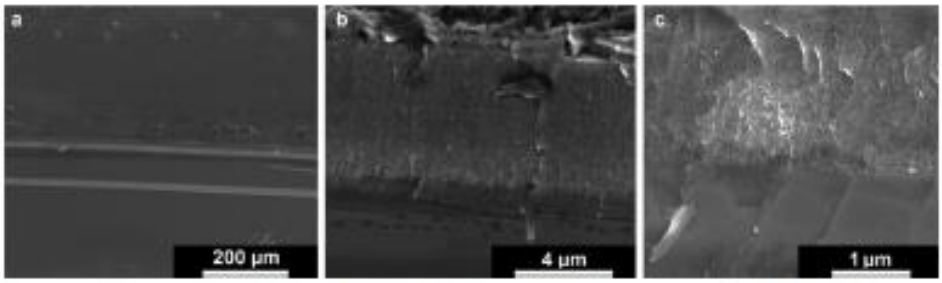

Fig. 9. SEM observations at different magnifications of a pSi sample after 150 galvanostatic cycles at 300 µA cm^{-2} with cut-off voltages of 0.1 V and 2 V.

Galvanostatic cycling at different current rates with cut-off voltages of 0.1 V and 2 V is displayed in Figure 10. Although a decrease of the capacity was observed when the current was increased, the capacity remained stable for a decade of cycles at each rate, at current densities of 100 µA cm^{-2} (~ C/27), 150 µA cm^{-2} (~ C/18), 200 µA cm^{-2} (~ C/14), 250 µA cm^{-2} (~ C/11), 300 µA cm^{-2} (~ C/9), 400 µA cm^{-2} (~ C/7), and 500 µA cm^{-2} (~ C/5). No capacity fading was observed for these current densities. This rate capability test showed that the reversible capacity is decreasing when current rate increases, until the applied current

density reaches 750 µA cm^{-2}. At a current density higher than 500 µA cm^{-2}, here for 750 µA cm^{-2} (~ C/4), a strong decrease was observed. This behavior may be due to the limitation of solid state ion diffusion in the Si, that cannot permit Li to alloy the Si material in depth [13, 29, 30]. This apparent fading is not due to a loss or degradation of the material, as the capacity returned to its precedent value at a lower rate of 500 µA cm^{-2} (see Fig. 10).

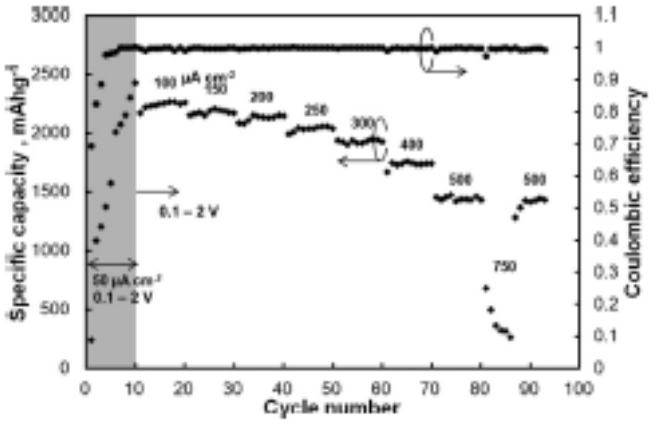

Fig. 10. Galvanostatic profiles of specific capacities (diamonds) and coulombic efficiency (circles) at different current densities for a Li/pSi half-cell with cut-off voltages of 0.1 V and 2 V.

4. Conclusion

A silicon-based negative electrode material has been prepared through an electrochemical etching process, achieving a mesoporous silicon layer of about 5 µm thick with pores diameter ranging form 60 to 70 nm . CV scanning showed that the intensity of the cathodic peak attributed to the lithiation of Si increased upon scanning, until it stabilized after the 50th cycle. This observation would monitor that lithiation and delithiation reactions are controlled by the Li diffusion in the depth of the pSi layer. SEM and EDX characterizations indeed showed that, for a sample cycled 10 times, there are two regions with two distinct morphologies in the porous layer and with different chemical compositions. Due to a slow penetration of the electrolyte inside the mesopores, only part of the pSi was involved in the lithiation-delithiation process, whereas the bottom of pores remained unaffected. In the bottom region of the pores, the absence of elements such as fluorine and phosphorous would assess this hypothesis, whereas these elements are present on the top part of the pSi

layer due to the electrolyte decomposition. In contrast, for a mesoporous sample cycled 50 times, fluorine is present in the bottom region of the pores, suggesting that the electrolyte could reach the whole porous silicon layer. Based on cyclic voltammetry experiments and EDX analysis of cycled samples, we suggest that the underneath wafer is not involved in lithiation/delithiation reactions. Galvanostatic cycling at a rate of 300 µA cm^{-2} with cut-off voltages of 0.07 and 2 V showed a specific capacity of 2480 mAh g^{-1} after 30 charge-discharge cycles; the capacity then faded for the 100 subsequent cycles. SEM observations showed that these galvanostatic conditions, with a lower cut-off voltage of 0.07 V, promoted mechanical damages in the porous layer. These damages would be due to the formation of a crystalline phase during the alloying charge, inducing strong volumetric changes. For the lower cut-off voltage of 0.1 V, the specific capacity was 1910 mAh g^{-1} with capacity retention of 97 % for 70 cycles. SEM observations showed that there are no mechanical damages due to the volumetric expansion even after 150 charge-discharge cycles. Thus, we validate our electrode architecture. Only the mesoporous Si layer is involved in the electrochemical reactions of lithiation and delithiation, while the underneath Si wafer remained unaffected even after long-time cycling. Mesoporous Si obtained from electrochemical etching of a Si wafer would be an efficient negative electrode material with high capacity for Li-ion batteries.

Acknowledgement

This work was supported by Région Centre, France, through BLaDES project, and by the French Gouvernment through the Investissements d'Avenir Tours2015 project.

References

[1] J.F.M. Oudenhoven, L. Baggetto, P.H.L. Notten, Advanced Energy Materials, 1 (2011) 10-33.

[2] R.W. Hart, H.S. White, B. Dunn, D.R. Rolison, Electrochemistry Communications, 5 (2003) 120-123.

[3] Y. He, X. Yu, G. Li, R. Wang, H. Li, Y. Wang, H. Gao, X. Huang, Journal of Power Sources, 216 (2012) 131-138.

[4] M. Green, E. Fielder, B. Scrosati, M. Wachtler, J.S. Moreno, Electrochemical and Solid-State Letters, 6 (2003) A75-A79.

[5] J.P. Maranchi, A.F. Hepp, P.N. Kumta, Electrochemical and Solid-State Letters, 6 (2003) A198-A201.

[6] T. Moon, C. Kim, B. Park, Journal of Power Sources, 155 (2006) 391-394.

[7] A. Arie, W. Chang, J. Lee, J Solid State Electrochem, 14 (2010) 51-56.

[8] P.R. Abel, Y.-M. Lin, H. Celio, A. Heller, C.B. Mullins, ACS Nano, 6 (2012) 2506-2516.

[9] H. Wu, G. Chan, J.W. Choi, I. Ryu, Y. Yao, M.T. McDowell, S.W. Lee, A. Jackson, Y. Yang, L. Hu, Y. Cui, Nat. Nano., 7 (2012) 310.

[10] A. Vlad, A.L.M. Reddy, A. Ajayan, N. Singh, J.-F. Gohy, S. Melinte, P.M. Ajayan, Proceedings of the National Academy of Sciences, (2012).

[11] D. Mazouzi, N. Delpuech, Y. Oumellal, M. Gauthier, M. Cerbelaud, J. Gaubicher, N. Dupré, P. Moreau, D. Guyomard, L. Roué, B. Lestriez, Journal of Power Sources, 220 (2012) 180-184.

[12] M. Thakur, M. Isaacson, S.L. Sinsabaugh, M.S. Wong, S.L. Biswal, Journal of Power Sources, 205 (2012) 426-432.

[13] X. Sun, H. Huang, K.-L. Chu, Y. Zhuang, Journal of Electronic Materials, 41 (2012) 2369-2375.

[14] H.-C. Shin, J.A. Corno, J.L. Gole, M. Liu, Journal of Power Sources, 139 (2005) 314-320.

[15] D.-K. Kang, J.A. Corno, J.L. Gole, H.-C. Shin, Journal of The Electrochemical Society, 155 (2008) A276-A281.

[16] V. Lehmann, Electrochemical Pore Formation, in: Electrochemistry of Silicon, Wiley-VCH Verlag GmbH, 2002, pp. 97-126.

[17] V. Lehmann, R. Stengl, A. Luigart, Materials Science and Engineering: B, 69–70 (2000) 11-22.

[18] C. Pereira-Nabais, J. Światowska, A. Chagnes, F. Ozanam, A. Gohier, P. Tran-Van, C.-S. Cojocaru, M. Cassir, P. Marcus, Applied Surface Science, (2012).

[19] J. Graetz, C.C. Ahn, R. Yazami, B. Fultz, Electrochemical and Solid-State Letters, 6 (2003) A194-A197.

[20] D. Aurbach, Y. Talyosef, B. Markovsky, E. Markevich, E. Zinigrad, L. Asraf, J.S. Gnanaraj, H.-J. Kim, Electrochimica Acta, 50 (2004) 247-254.

[21] C.K. Chan, R. Ruffo, S.S. Hong, Y. Cui, Journal of Power Sources, 189 (2009) 1132-1140.

[22] E. Luais, J. Sakai, S. Desplobain, G. Gautier, F. Tran-Van, F. Ghamouss, Journal of Power Sources, 242 (2013) 166-170.

[23] M. Dahbi, F. Ghamouss, F. Tran-Van, D. Lemordant, M. Anouti, Journal of Power Sources, 196 (2011) 9743-9750.

[24] X. Chen, K. Gerasopoulos, J. Guo, A. Brown, C. Wang, R. Ghodssi, J.N. Culver, Advanced Functional Materials, 21 (2011) 380-387.

[25] L. Baggetto, R.A.H. Niessen, F. Roozeboom, P.H.L. Notten, Advanced Functional Materials, 18 (2008) 1057-1066.

[26] B. Laïk, D. Ung, A. Caillard, C. Sorin Cojocaru, D. Pribat, J.-P. Pereira-Ramos, J Solid State Electrochem, 14 (2010) 1835-1839.

[27] L.-F. Cui, R. Ruffo, C.K. Chan, H. Peng, Y. Cui, Nano Letters, 9 (2008) 491-495.

[28] M.N. Obrovac, L. Christensen, Electrochemical and Solid-State Letters, 7 (2004) A93-A96.

[29] Y. Oumellal, N. Delpuech, D. Mazouzi, N. Dupre, J. Gaubicher, P. Moreau, P. Soudan, B. Lestriez, D. Guyomard, Journal of Materials Chemistry, 21 (2011) 6201-6208.

[30] S. Rousselot, M. Gauthier, D. Mazouzi, B. Lestriez, D. Guyomard, L. Roué, Journal of Power Sources, 202 (2012) 262-268.

Figure Captions

Figure 1 – Cross-sectional SEM images of a mesoporous Si wafer in (a) low magnification and (b) high magnification.

Figure 2 - Cyclic voltammograms of pSi negative electrodes in EC/DMC + 1M $LiPF_6$ at a scan rate of 0.1 mV s^{-1}. (a) 1st cycle for pSi material with native oxide (bold curve) and for pSi after a HF treatment (dashed curve). (b) 1st cycle (bold curve), 2nd cycle (dashed curve) and 3rd cycle (dotted curve) for an as-prepared sample. (c) 1st cycle (bold curve), 10th cycle (dashed curve), and 50th cycle (dotted curve) for an as-prepared sample. (d) Peak intensity of the cathodic peak related to the lithiation of pSi.

Figure 3 - Cyclic voltammograms of a pSi negative electrode in EC/DMC + 1M $LiPF_6$ at a scan rate of 0.1 mV s^{-1}. (a) 10th cycle (bold continuous curve), 15th cycle (dashed curve), 20th cycle (dotted curve) and 30th cycle (thin continuous curve). (b) 11th to 25th cycles in a potential window from 0.02 to 1 V.

Figure 4 – (a) SEM image in a tilted view of the mesoporous Si after 10 cycles with (i) the surface of the pSi (ii) main part of pSi affected by the electrolyte penetration for 10 CVs (iii) pSi part unaffected by the electrochemical reactions. Schematic of regions in the SEM image is shown on the right. (b) EDX spectra collected from the (i) pSi surface, (ii) main part of the pSi and (iii) bottom of the pSi pores.

Figure 5 – (a) SEM image in a tilted view of the mesoporous Si after 50 cycles with (i) the surface of the pSi (ii) main part of pSi layer (iii) bottom of the porous layer. Schematics of regions in the SEM image is shown on the right. (b) EDX spectra achieved from the (i) pSi surface, (ii) main part of the pSi and (iii) bottom of the pSi.

Figure 6 - Galvanostatic profiles of specific capacities (diamonds) and coulombic efficiency (circles) for a Li/pSi half-cell with cut-off voltages of 0.07 V and 2 V.

Figure 7 - SEM observations at different magnifications of a pSi sample after 150 galvanostatic cycles at 300 µA cm^{-2} with cut-off voltages of 0.07 V and 2 V.

Figure 8 - Galvanostatic profiles of specific capacities (diamonds) and coulombic efficiency (circles) for a Li/pSi half-cell with cut-off voltages of 0.1 V and 2 V.

Figure 9 - SEM observations at different magnifications of a pSi sample after 150 galvanostatic cycles at 300 µA cm^{-2} with cut-off voltages of 0.1 V and 2 V.

Figure 10 - Galvanostatic profiles of specific capacities (diamonds) and coulombic efficiency (circles) at different current densities for a Li/pSi half-cell with cut-off voltages of 0.1 V and 2 V.